Trafficking activity of myosin XXI is required in assembly of *Leishmania* flagellum

Santharam S. Katta[1,*], Trinadh V. Satish Tammana[1,*], Amogh A. Sahasrabuddhe[1,*], Virendra K. Bajpai[2] and Chhitar M. Gupta[1,‡]

[1]Molecular and Structural Biology Division, [2]Electron Microscopy Unit, Central Drug Research Institute, C.S.I.R., Uttar Pradesh, Lucknow-226001, India

*These authors contributed equally to this work
‡Author for correspondence (drcmg@rediffmail.com)

Accepted 29 March 2010
Journal of Cell Science 123, 2035-2044

doi:10.1242/jcs.064725

Summary

Actin-based myosin motors have a pivotal role in intracellular trafficking in eukaryotic cells. The parasitic protozoan organism *Leishmania* expresses a novel class of myosin, myosin XXI (Myo21), which is preferentially localized at the proximal region of the flagellum. However, its function in this organism remains largely unknown. Here, we show that Myo21 interacts with actin, and its expression is dependent of the growth stage. We further reveal that depletion of Myo21 levels results in impairment of the flagellar assembly and intracellular trafficking. These defects are, however, reversed by episomal complementation. Additionally, it is shown that deletion of the *Myo21* gene leads to generation of ploidy, suggesting an essential role of Myo21 in survival of *Leishmania* cells. Together, these results indicate that actin-dependent trafficking activity of Myo21 is essentially required during assembly of the *Leishmania* flagellum.

Key words: Trypanosomatids, Intraflagellar transport, Myosin, Trafficking

Introduction

Myosin proteins constitute a group of actin-based molecular motors that produce movement along the actin filaments and have diverse motile functions in eukaryotic cells, ranging from muscle contraction and pseudopodal motility, to vesicle transport and cytokinesis (Woolner and Bement, 2009). These proteins share a common domain plan, consisting of N-terminal head domain (motor domain) responsible for actin binding and ATPase activity, a light-chain-binding neck domain, and a C-terminal tail domain that imparts functional specificity to different classes of myosins (Krendel and Mooseker, 2005). Owing to a high degree of sequence conservation in the head domain, myosin has been anticipated to power their movements along F-actin tracks, whereas divergent tail domains bind a diverse array of partners, including proteins and membranes (Karcher et al., 2002). Based on variations in the amino-acid sequence and domain composition, myosins have been classified into more than 30 classes in different organisms (Odronitz and Kollmar, 2007; Foth et al., 2006). Genomes of kinetoplastid parasites, such as *Trypanosoma* and *Leishmania*, encode a class of myosins (El-Sayeed et al., 2005) that were classified as myosin XXI (Myo21) by Foth and co-workers (Foth et al., 2006). Myo21, unlike other myosin proteins, contains UBA-like protein domains and has no structural or functional relationship with the myosins present in other organisms possessing cilia or flagella (Odronitz and Kollmar, 2007; Foth et al., 2006).

Leishmania are a group of trypanosomatid parasites that cause a number of life-threatening human diseases including ‘Kala-azar’ (Desjeux, 2004). These parasites mainly exist in two forms: (1) the non-motile amastigote, residing within the mammalian macrophages, and (2) highly motile promastigotes, which reside in the alimentary tract of the sandfly vector. The amastigote forms possess only rudimentary flagella, whereas the promastigote forms actively swim using their single long flagellum. The basic scaffold of the eukaryotic flagellum consists of nine characteristically arranged outer microtubule doublets encircling two central-pair microtubules that are interlinked with several discrete substructures, such as radial spokes, inner and outer dynein arms, nexins and other intricacies ascribing specific flagellar functions. This structure in trypanosomatids, including *Leishmania*, shows an increased complexity, because as well as the axoneme, it also contains an extra-axonemal protein lattice known as the paraflagellar rod (PFR). The PFR runs along the entire length of the flagellum and is crucial for cell motility in trypanosomatids (Santrich et al., 1997).

In *Trypanosoma*, yet another subflagellar structure has been described: a transmembrane mobile junction, known as a flagella connector (FC). This structure connects the tip of the growing flagellum with the old one during cell division (Moreira-Leite et al., 2001; Briggs et al., 2004). The flagellum in these organisms is attached to the cell body through the basal body, and its membrane is continuous with a cup-shaped membrane invagination, called the flagellar pocket (Field and Carrington, 2009).

The flagellum, in general, is a dynamic microtubule-based cellular protrusion that imparts motility and/or sensory functions associated with a range of biological processes related to human health. The dynamics of flagella involve a process of assembly and disassembly, the knowledge of which is now beginning to emerge. This process requires movements of protein cargoes from the flagellum base to its tip (anterograde) and also from the tip to its base (retrograde) and is termed as ‘intraflagellar transport’ (IFT) (Rosenbaum and Witman, 2002). Based on the existing knowledge, IFT is powered by the microtubule-based motor proteins such as kinesin II and dynein complexes for anterograde and retrograde transports, respectively (Cole and Snell, 2009). However, the flagella of trypanosomes and *Leishmania* as well as containing microtubule-based axonemal structures also contain PFRs, but the mechanism by which the PFR proteins are transported and

Journal of Cell Science

assembled within the flagellar compartment remains unknown. Furthermore, the FC (flagella connector) has been shown to move beyond the axoneme, even in the absence of IFT (Kohl et al., 2003; Davidge et al., 2006). It thus appears that the existing knowledge of the transport of proteins into and within the flagellar compartment is still incomplete.

In addition to microtubules and microtubule-based motor proteins, the flagellar compartment also contains actin, actin-related proteins and actin-binding proteins in a variety of organisms (Muto et al., 1994; Yanagisawa and Kamiya, 2001; Ersfeld and Gull, 2001; Sahasrabuddhe et al., 2004; Minoura, 2005; Broadhead et al., 2006). However, little is known about the functions of the actin-based cytoskeletal elements in the flagellum. In flagella of *Chlamydomonas*, actin has been reported to form an important subunit of the inner-arm dynein (Kato-Minoura et al., 1997; Hayashi et al., 2001). In addition, the actin-dynamics-regulating protein ADF/cofilin (Cof), has recently been shown to be involved in assembly of the *Leishmania* flagellum (Tammana et al., 2008), suggesting a role of actin dynamics in this process. As the *Leishmania* flagellum, besides containing actin and Cof (Sahasrabuddhe et al., 2004; Tammana et al., 2008) also contains Myo21 (Katta et al., 2009), we speculate that actomyosin-based transport of flagellar proteins might also be required during flagellum assembly. To test this possibility, we analyzed the effects of *Myo21* gene deletion on flagellum assembly and intracellular transport in *Leishmania* cells. Our results show that Myo21 is essentially required in both flagellar assembly and cell survival.

Results

Myo21 associates with actin in *Leishmania* cells

The *Leishmania* genome encodes two myosin genes: one that corresponds to class I myosin, whereas the other is a novel class of myosin, myosin XXI (Myo21) (Foth et al., 2006). However, our recent studies have shown that *Leishmania* express only Myo21, which, in the promastigotes is largely concentrated in the proximal region of the flagellum, with a diffuse distribution in other flagellar and cell-body compartments (Katta et al., 2009). This differential Myo21 distribution has now been confirmed by comparing the localization of Myo21 in *Leishmania* promastigotes before and after NP-40 treatment (supplementary material Fig. S1). As this protein has also been reported to partially colocalize with actin in *Leishmania* cells (Katta et al., 2009), we reanalyzed the Myo21 association with actin using immunofluorescence microscopy and co-immunoprecipitation techniques.

As myosins interact only with the filamentous form of actin, which is infrequently seen in *Leishmania* cells, compared with eukaryotic cells (Nayak et al., 2005), we mainly focused on the cells that clearly showed actin filaments or patches. Myo21 colocalized with actin in such cells (Fig. 1A; also see supplementary material Fig. S1) although the extent of Myo21 signal varied from cell to cell. To analyze whether actin interacts with the head domain or tail domain of Myo21, the promastigotes that expressed GFP conjugates of H-Myo21 (head domain) and T-Myo21 (tail domain) along with full length Myo21 (Katta et al., 2009) were used in immunoprecipitation experiments (Fig. 1B). The cells were first lysed with Triton X-100 (1% v/v) and clear detergent-soluble fractions were subjected to immunoprecipitation using anti-GFP antibodies. Analysis of the immunoprecipitates revealed that actin co-immunoprecipitated with full-length Myo21 and H-Myo21, but not with T-Myo21 (Fig. 1C). These results not only confirmed the existence of acto-Myo21 complexes in *Leishmania* promastigotes

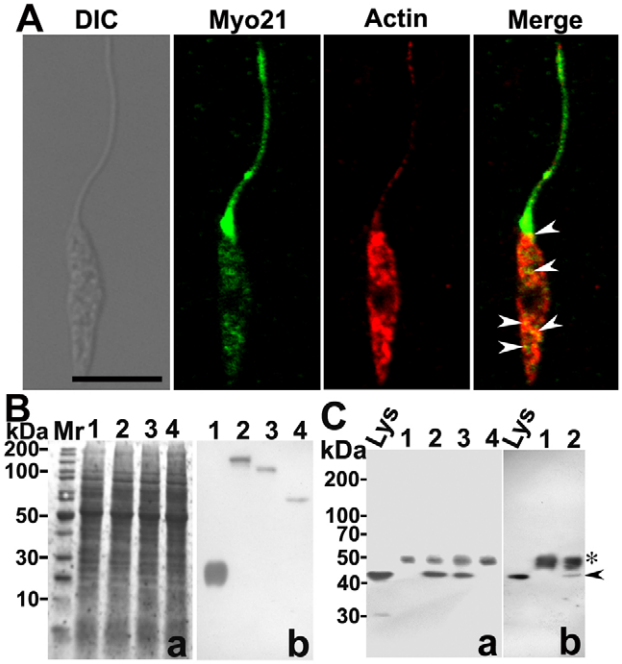

Fig. 1. Interaction of Myo21 with actin. (**A**) Immunofluorescence images at increased gain and laser intensity showing colocalization of Myo21 (green) with actin (red) in *Leishmania* promastigotes. Arrowheads indicate co-localization of Myo21 with actin in the cell body. Scale bar: 5 µm. (**B**) Expression analyses of *Leishmania* cells expressing GFP (lane 1), Myo21-GFP (lane 2), H-Myo21-GFP (lane 3) and T-Myo21-GFP (lane 4) (40 µg protein/lane). a, Coomassie Blue stained PVDF membrane; b, western blot of membrane using anti-GFP antibodies. (**C**) Immunoprecipitation analyses by western blotting. a, Western blot of immunoprecipitates obtained from the cleared lysates (~3 mg/ml protein) of *Leishmania* promastigotes expressing GFP alone (lane 1), Myo21-GFP (lane 2), H-Myo21-GFP (lane 3) and T-Myo21-GFP (lane 4), using anti-GFP antibodies (2 µg in 1 ml lysates), and probed with anti-*Leishmania* actin antibodies (30 µl of 200 µl total immunoprecipitate per lane). b, Western blot of immunoprecipitate obtained from cleared lysate (~2.2 mg/ml protein) of axenic amastigotes expressing GFP alone (lane 1) and Myo21-GFP (lane 2) using anti-GFP antibodies (2 µg in 1 ml lysate) and probed with anti-actin antibodies (30 µl of 100 µl total immunoprecipitate per lane). *, Antibody heavy chain; arrowhead, actin; Lys, cleared cell lysate (1% input).

but also revealed that the head domain of Myo21 was responsible for its interactions with actin.

Myo21 expression is growth specific and correlates with flagellar length

Flagellar length in *Leishmania* is closely linked to the cell life cycle and growth phase (Cuvillier et al., 2003; Zakai et al., 1998), with flagella twice the length of the cell body in metacyclic promastigotes and a short rudimentary flagellum in amastigotes (Rogers et al., 2002). As Myo21 expression depends on the parasite life cycle (Katta et al., 2009), we also examined whether this expression varied with the parasite growth phase. Interestingly, Myo21 expression levels increased gradually up to ~4.5-fold with the lowest in the early-log phase and the highest in the stationary phase (Fig. 2A). This was confirmed by measuring mRNA levels using semi-quantitative RT-PCR (supplementary material Fig. S2). This difference in the Myo21 expression levels between the different growth phases was also apparent in immunofluorescence

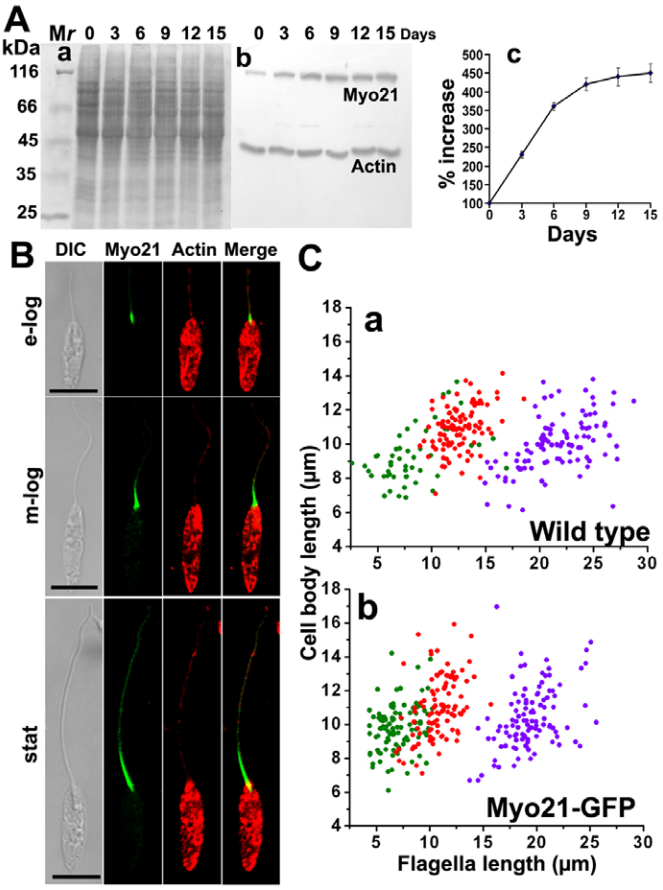

Fig. 2. Differential expression of Myo21 in different growth phases of *Leishmania* promastigotes and its correlation with flagellar length. (**A**) Western blot analysis of wild-type promastigotes harvested at different time intervals after their seeding to 10^5 cells/ml cell density from an early-log-phase culture (40 μg protein per lane). a, Ponceau-stained nitrocellulose membrane; b, western blot of membrane probed with anti-Myo21 and anti-*Leishmania* actin antibodies; c, densitometric analysis of Myo21 bands normalized with respective actin band, showing a gradual increase in the expression levels of Myo21. Values shown are means ± s.d. of three experiments. (**B**). Immunofluorescence images of *Leishmania* promastigotes labeled for Myo21 (green) and *Leishmania*-actin (red) at three different growth phases; e-log, early-log phase; m-log, mid-log phase; stat, stationary phase. Images were collected at the same settings of gain and offset, and lower laser intensities under the confocal microscope to show relative abundance of Myo21 at the proximal region of the flagellum. Scale bar: 5 μm. A gradual increase in the fluorescence intensities of Myo21 in flagella of mid-log and stationary phase cells compared with early-log-phase cells corroborate the results of the western blot analysis in A. (**C**) Analysis of flagellar length versus body length of *Leishmania* promastigotes at early-log (green), mid-log (red) and stationary phases (purple) of growth. a, Wild-type cells; b, Myo21-GFP-expressing cells. A total of 100 cells were measured in each case.

images of the promastigotes at the proximal region (Fig. 2B). However, no difference in actin staining was observed in different growth phases of these parasites. To examine whether Myo21 expression correlated with the flagellar length, we analyzed about 100 cells each from the early-log, mid-log and stationary phases. The average flagellar length in stationary phase cells was about threefold and twofold higher than that of the early-log and mid-log phase cells, respectively, without any significant change in the body lengths (Fig. 2Ca). To further analyze whether increase in the Myo21 expression directly affected the flagellar length, we measured the flagellar lengths in Myo21-GFP-overexpressing *L. donovani* cells (Katta et al., 2009) at different phases of their growth; no significant differences in the flagellar length was observed compared with normal cells (Fig. 2C,b). These results indicate that the Myo21 is perhaps not directly involved in regulation of flagellar length during the stage differentiation in *Leishmania* promastigotes.

Myo21 is essentially required for survival of *Leishmania* cells

To investigate the role of Myo21 in assembly of *Leishmania* flagellum as well as in other cellular processes, we knocked out the *Myo21* gene in *L. donovani* promastigotes. Genome sequence data of *L. major*, *L. infantum* and *L. braziliensis* have revealed single-copy architecture of the *Myo21* gene in their genomes (www.genedb.org), which we also confirmed in our *L. donovani* strain (supplementary material Fig. S3). As it is a diploid organism, *L. donovani* carries two myosin alleles. To replace both these alleles, two gene deletion constructs were prepared with different antibiotic-resistance markers: neomycin phosphotransferase (*Neo*) and hygromycin phosphotransferase (*Hyg*) genes, which confer resistance to the antibiotics G-418 and hygromycin B, respectively. Deletion constructs contained 950 bp upstream and 1200 bp downstream regions of the *Myo21* gene at the 5′ and 3′ ends of the antibiotic-resistance genes, respectively (Fig. 3A).

Both the *Neo* and *Hyg* cassettes were separately transfected in *L. donovani* promastigotes by electroporation and antibiotic-resistant clones were selected on DMEM-agar plates containing G-418 or hygromycin B (10 μg/ml each). These clones were then analyzed for the replacement of *Myo21* allele by Southern blotting using *Neo* or *Hyg* gene probes. All the colonies screened (more than 50) from both the G-418 and hygromycin plates were found to have integration of deletion cassettes at the *Myo21* gene locus and Southern blots of one clone each from G-418- and hygromycin-resistant colonies are shown (Fig. 3B). Western blot analysis showed approximately 40-50% depletion of Myo21 levels in these clones (Fig. 3C). To obtain a *Myo21*-null mutant, the hygromycin resistant heterozygous clone was subjected to a second round of transfection with the neomycin construct. Clones selected on the DMEM-agar plates containing G-418 and hygromycin B (10 μg/ml each) were subsequently analyzed by both Southern and western blotting. To our surprise, despite replacement of both the alleles by *Hyg* and *Neo* genes (a total of 100 colonies screened), *Myo21*-null mutants could not be obtained (Fig. 3B,C, also see supplementary material Fig. S4). Expression levels of Myo21 in double allele-replaced mutants ($Myo21^{-/-}$) were however comparable with the heterozygous clones having only single allele replacement (Fig. 3C), and was consistent in five randomly selected $Myo21^{-/-}$ clones (supplementary material Fig. S4). Furthermore, flow-cytometric analysis showed no gross change in the DNA content of the $Myo21^{-/-}$ clones compared with wild-type and $Myo21^{+/-}$ cells (supplementary material Fig. S4), suggesting generation of aneuploidy in the $Myo21^{-/-}$ clones. As ploidy generation in *Leishmania* has been viewed as a measure of essentiality of genes (Mottram et al., 1996; Cruz et al., 1993; Dumas et al., 1997; Tovar et al., 1998), Myo21 expression can be regarded essential for survival of the *Leishmania* cells in culture. In the absence of $Myo21^{-/-}$ mutants, we episomally expressed Myo21-GFP (Katta et al., 2009) in one of the hygromycin-B-resistant heterozygous clones ($Myo21^{+/-}$) for add-back analyses (Fig. 3D). The $Myo21^{+/-}$ cells

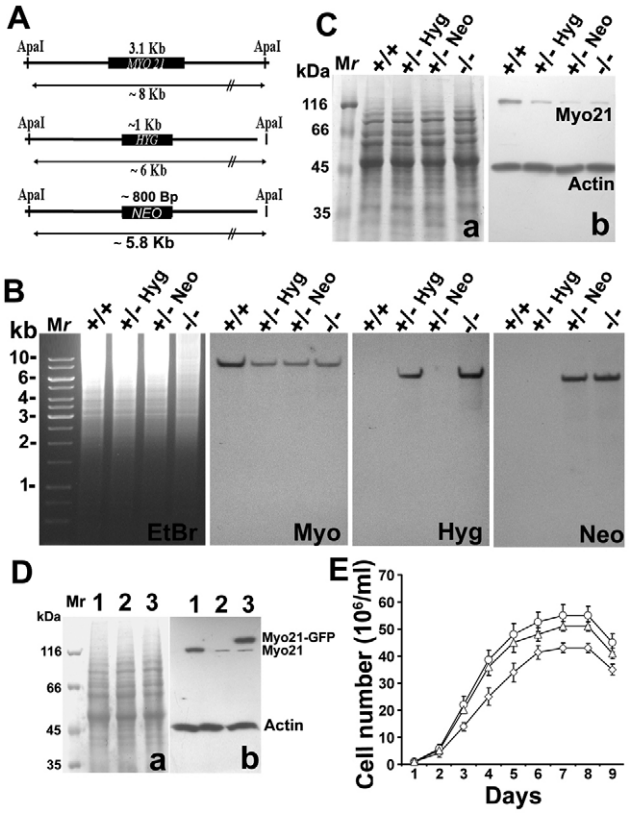

Fig. 3. Deletion of *Myo21* gene. (**A**) Schematic representation of *Myo21* locus in *L. donovani* showing size differences before and after integration of *Neo* or *Hyg* cassettes after restriction digestion by *Apa*I. (**B**) Southern blot analysis of the *Myo21*$^{+/-}$ and *Myo21*$^{-/-}$ mutants confirming replacement of *Myo21* alleles. Signal of Myo21 in *Myo21*$^{-/-}$ homozygous mutant indicates ploidy generation. EtBr, ethidium bromide; Myo, Hyg and Neo, southern blots probed with *Myo21*, *Hyg* and *Neo* gene probes, respectively. (**C**) Western blot analysis of wild-type (*Myo21*$^{+/+}$), *Myo21*$^{+/-}$*Hyg*, *Myo21*$^{+/-}$*Neo* and *Myo21*$^{-/-}$ cells in the mid-log phase showing depletion of Myo21 in heterozygous as well as in homozygous mutants. a, Coomassie-Blue-stained PVDF membrane (40 µg protein per lane); b, western blot using anti-Myo21 and anti-*Leishmania* actin antibodies. (**D**) Expression analysis of Myo21-GFP in *Myo21*$^{+/-Comp}$ cells in the mid-log phase. a, Ponceau-stained nitrocellulose membrane (40 µg protein per lane); b, western blot probed with anti-Myo21 and anti-*Leishmania* actin antibodies. Lane 1, wild type; lane 2, *Myo21*$^{+/-}$; lane 3, *Myo21*$^{+/-Comp}$. (**E**) Growth analysis of wild type (circles), *Myo21*$^{+/-}$ (diamonds), and *Myo21*$^{+/-}$ and *Myo21*$^{+/-Comp}$ cells (triangles). Calculated generation time (in hours) for wild type, 10.40±0.45; *Myo21*$^{+/-}$ cells, 13.05±0.70; *Myo21*$^{+/-Comp}$, 11.20±0.5. +/+, wild-type cells; +/–Hyg, hygromycin-resistant heterozygous *Myo21* mutant; +/–Neo, neomycin-resistant heterozygous *Myo21* mutant; –/–, homozygous *Myo21* mutant.

exhibited slightly reduced growth, which was restored to normal upon episomal complementation with Myo21-GFP (*Myo21*$^{+/-Comp}$) (Fig. 3E). However, H-Myo21-GFP or T-Myo21-GFP failed to complement *Myo21*$^{+/-}$ cells, suggesting that both the head and the tail domains are essentially required for Myo21 function.

Reduction in Myo21 levels results in reduced flagellar length and absence of PFRs

Both the single and double mutants appeared to have similar expression levels of Myo21. Therefore, one of the hygromycin-B-resistant heterozygous clones (*Myo21*$^{+/-}$) was used for detailed

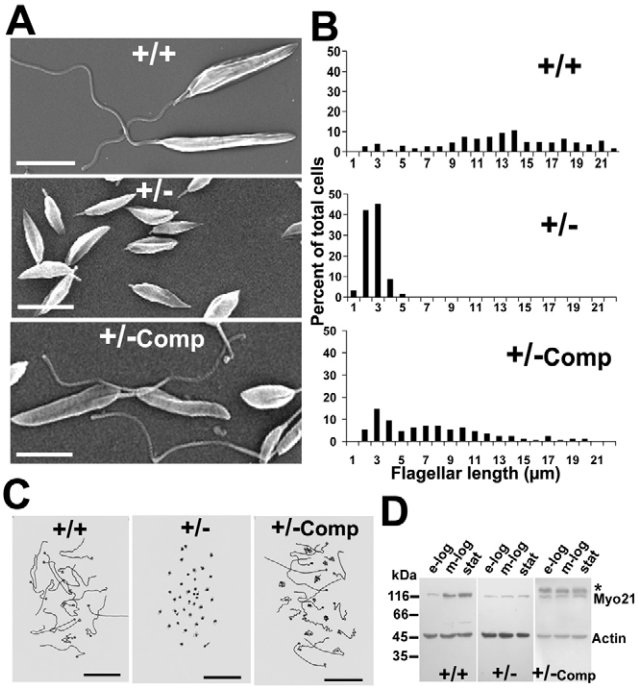

Fig. 4. Analysis of cell shape, flagellar length, motility and Myo21 expression in *Myo21* mutants. (**A**) Scanning electron microscopy images showing stumpy cell body and reduced flagellar length of *Myo21*$^{+/-}$ (+/–) cells, which reverted back to normal in *Myo21*$^{+/-Comp}$ (+/–Comp) cells. Scale bars: 5 µm. (**B**) Histograms of flagellar length of wild-type (+/+), *Myo21*$^{+/-}$ (+/–) and *Myo21*$^{+/-Comp}$ (+/–Comp) cells. More than 200 cells were analyzed from each cell line. (**C**) Motility analysis of *Myo21* mutants by time-lapse microscopy. Traced paths of live, individual cells from a time-lapse movie of 36 seconds, showing non-motile nature of *Myo21*$^{+/-}$ (+/–) cells compared with wild-type (+/+) cells and attainment of normal motility in *Myo21*$^{+/-Comp}$ (+/–Comp) cells. Scale bars: 100 µm. (**D**) Western blot analysis of the wild type (+/+), *Myo21*$^{+/-}$ (+/–) and *Myo21*$^{+/-Comp}$ (+/–Comp) cells showing the absence of growth-dependent increase in Myo21 levels in *Myo21*$^{+/-}$ and *Myo21*$^{+/-Comp}$ cells (40 µg protein per lane). Actin, internal loading control; *, Myo21-GFP; e-log, early-log-phase cells; m-log, mid-log-phase cells; stat, stationary-phase cells.

analyses throughout the present study and wherever necessary, more clones were included for confirmation of the results. Since Myo21 expression levels varied with cell growth, all the analyses were done strictly using ‘mid-log-phase’ cells (supplementary material Fig. S5), unless specifically stated otherwise. Overall, the heterozygous mutants appeared short and stumpy (Fig. 4A), and possessed significantly reduced flagellar lengths averaging 2.13±1.65 µm (*n*=200), compared with 12.40±4.97 µm (*n*=204) in the wild-type cells (Fig. 4B; also see supplementary material Fig. S6). The short flagella in *Myo21*$^{+/-}$ cells exhibited occasional bending movements, which were not enough to propel the cell forward (Fig. 4C; also see supplementary material Movie 1). Since wild-type cells exhibited variable expression of Myo21 at different stages, it was essential to examine whether the same was true for *Myo21*$^{+/-}$ cells. However, no significant change in the flagellar length with the growth stage was observed in the mutant cells (Fig. 4D). Myo21 expression also remained unchanged in different growth phases of *Myo21*$^{+/-Comp}$ cells. These results further confirm that Myo21 expression is not directly involved in growth-phase-specific regulation of flagellar length.

Immunofluorescence analysis of *Myo21*$^{+/-}$ cells showed the presence of Myo21, with a dot-like appearance at the proximal region of the rudimentary flagellum (supplementary material Fig. S7A). To examine whether relative distribution of Myo21 in NP-40-insoluble and -soluble fractions was altered in *Myo21*$^{+/-}$ cells, compared with wild-type cells, we analyzed these fractions by western blotting; no difference in the relative distributions of Myo21 was observed between the mutants and wild-type cells (supplementary material Fig. S7B).

The trypanosomatid flagellum is marked by an additional structure called the PFR (Bastin et al., 1996). We, therefore, examined the expression and location of PFR proteins in *Myo21*$^{+/-}$ cells using mAb2E10 antibodies, which detect major PFR proteins, i.e. PFR1 and PFR2, in the flagellum of *Leishmania* promastigotes (Ismach et al., 1989). Unlike wild-type *Leishmania* promastigotes, no PFR staining was seen in *Myo21*$^{+/-}$ cells (Fig. 5A). Further analysis revealed that in contrast to the wild-type cells, expression levels of the PFR proteins were undetectable in *Myo21*$^{+/-}$ cells, which were restored to normal by episomal complementation (Fig. 5B). Transmission electron microscopy revealed that the PFR structure was altogether absent in the flagella of *Myo21*$^{+/-}$ cells (Fig. 5C). Nevertheless, the canonical 9+2 arrangement of the axoneme microtubules appeared intact and no accumulation of vesicles or electron-dense particles could be seen in the flagellar ultrastructure of *Myo21*$^{+/-}$ cells (Fig. 5C). Importantly, the PFR was regained after episomal complementation with Myo21-GFP. These results suggest that Myo21 is essentially required in flagellar assembly and elongation in *Leishmania*.

Myo21$^{+/-}$ cells are defective in intracellular trafficking

Transmission electron microscopy analyses of about 90% of cross-sections of *Myo21*$^{+/-}$ cells through the flagellar pocket revealed that the flagellar pockets were 3-4 times larger (750-1200 nm diameter, *n*=62, 57/62) compared with wild-type cells (280-340 nm diameter, *n*=59) (Fig. 6), suggesting a defect in vesicular transport (Garcia-Salcedo et al., 2004; Allen et al., 2003) in these cells. To confirm this observation, we analyzed the transport of endocytic vesicles in *Leishmania* promastigotes by using the fluorophore N-(3-triethylammoniumpropyl)-4-{6-[4-(diethylamino)phenyl]-hexatrienyl}pyridinium dibromide (FM4-64), which has been widely used as a marker for assessing the flagellar-pocket activity in trypanosomatids (Sahin et al., 2008; Mullin et al., 2001). In wild-type cells, flagellar pockets were typically marked at 4°C, and the fluorophore efficiently endocytosed and trafficked down to form a characteristic multivesicular tubule (Ghedin et al., 2001) at 25°C within 1 hour (Fig. 7A). By contrast, in about 56% of *Myo21*$^{+/-}$ cells (*n*=660, 294/660), the fluorophore remained associated with the flagellar pocket and failed to get endocytosed under identical conditions. These results were verified independently in a total of four randomly selected heterozygous clones (two clones each from hygromycin B selectants and G-418 selectants) (supplementary material Fig. S8). After 2 hours, little accumulation of fluorophore above the kinetoplast region could be observed in these cells (Fig. 7A). Interestingly, about 37% (109 cells out of 294 cells that failed to traffic the endocytosed dye) of such *Myo21*$^{+/-}$ cells showed fluorophore accumulation in a crescent form at the flagellar-pocket region, which, to some extent, resembled the 'big-eye' phenotype, indicating defective endocytosis (Allen et al., 2003). This feature corresponded well with the excessive enlargement of some of the flagellar pockets (12%, 7 out of 57 enlarged flagellar pockets) observed during ultrastructural analyses (Fig. 6).

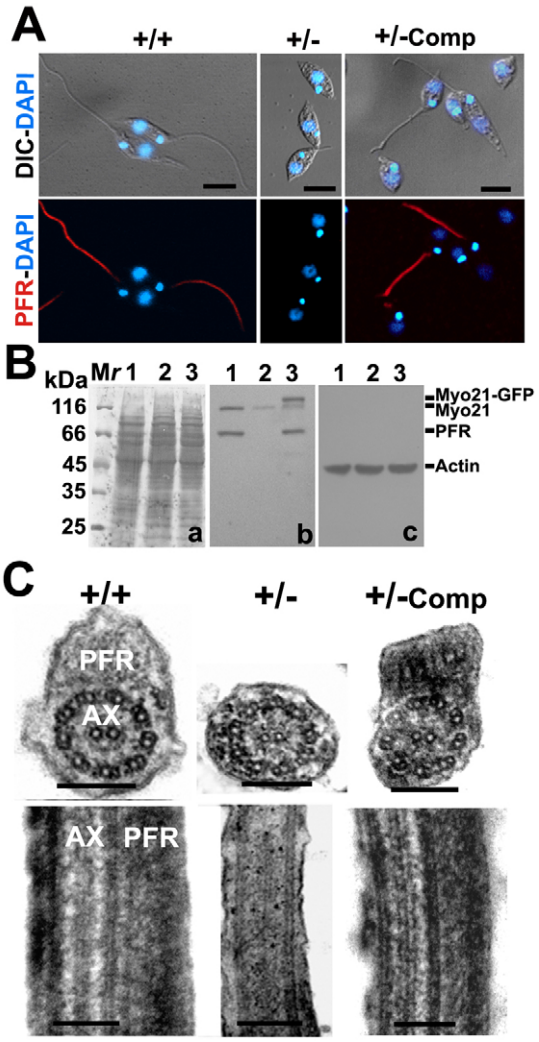

Fig. 5. Analysis of PFR in wild-type, *Myo21*$^{+/-}$ and *Myo21*$^{+/-Comp}$ cells. (**A**) Immunofluorescence images of wild-type (+/+), *Myo21*$^{+/-}$ (+/–) and *Myo21*$^{+/-Comp}$ (+/–Comp) cells, labeled for paraflagellar rod (PFR, red), showing absence of PFR in *Myo21*$^{+/-}$ cells, which was regained in *Myo21*$^{+/-Comp}$ cells. Nuclei and kinetoplasts are labeled with DAPI (cyan). Scale bars: 5 µm. (**B**) Western blot analysis of PFR protein expression in *Myo21*$^{+/-}$ cells. Lane 1, wild-type cells; lane 2, *Myo21*$^{+/-}$ cells; lane 3, Myo21$^{+/-Comp}$ cells, showing presence, absence and regain of PFR proteins, respectively. a, Coomassie-blue-stained PVDF membrane (40 µg protein per lane); b, western blot using anti-Myo21 and anti-PFR antibodies; c, western blot using anti-*Leishmania* actin antibodies after stripping. (**C**) Transmission electron micrographs of thin sections of the cells showing presence, absence and regain of PFR in wild type (+/+), *Myo21*$^{+/-}$ (+/–) and *Myo21*$^{+/-Comp}$ (+/–Comp) cells, respectively. PFR, paraflagellar rod; AX, axoneme. Scale bars: 100 µm. A total of 55 cross-sections (CSs) and 14 longitudinal sections (LSs) of wild-type cells, 47 CSs and 6 LSs of *Myo21*$^{+/-}$ cells, and 13 CSs and 7 LSs of *Myo21*$^{+/-Comp}$ cells were analyzed.

As an additional marker for intracellular trafficking, we also estimated secreted acid phosphatase (SAP) activity, which has been widely used for assessing the exocytic activity in these organisms (Overath et al., 1997; Cuvillier et al., 2000). SAP activity in the culture supernatants of the *Myo21*$^{+/-}$ mutant was significantly

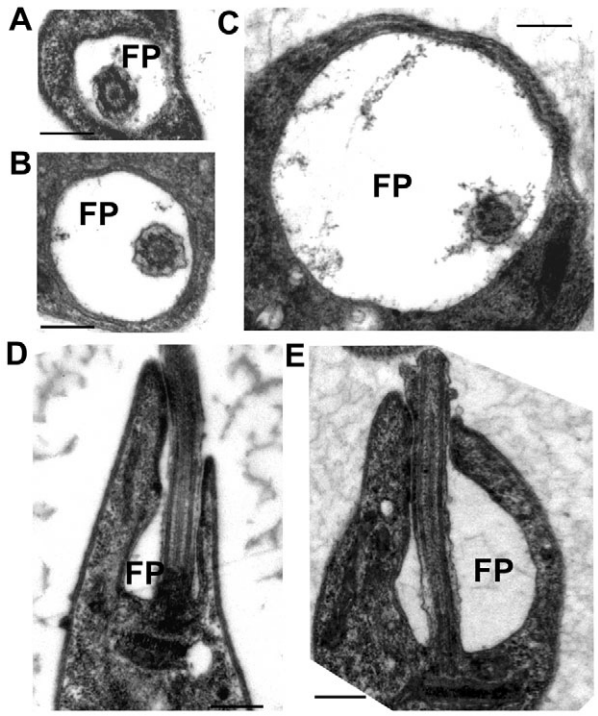

Fig. 6. Transmission electron micrographs showing the size of flagellar pockets. Cross-section (**A**) and longitudinal section (**D**) through the flagellar pocket of wild-type cell; cross-sections (**B** and **C**), and longitudinal section (**E**) of *Myo21*$^{+/-}$ cells. Scale bars: 200 nm.

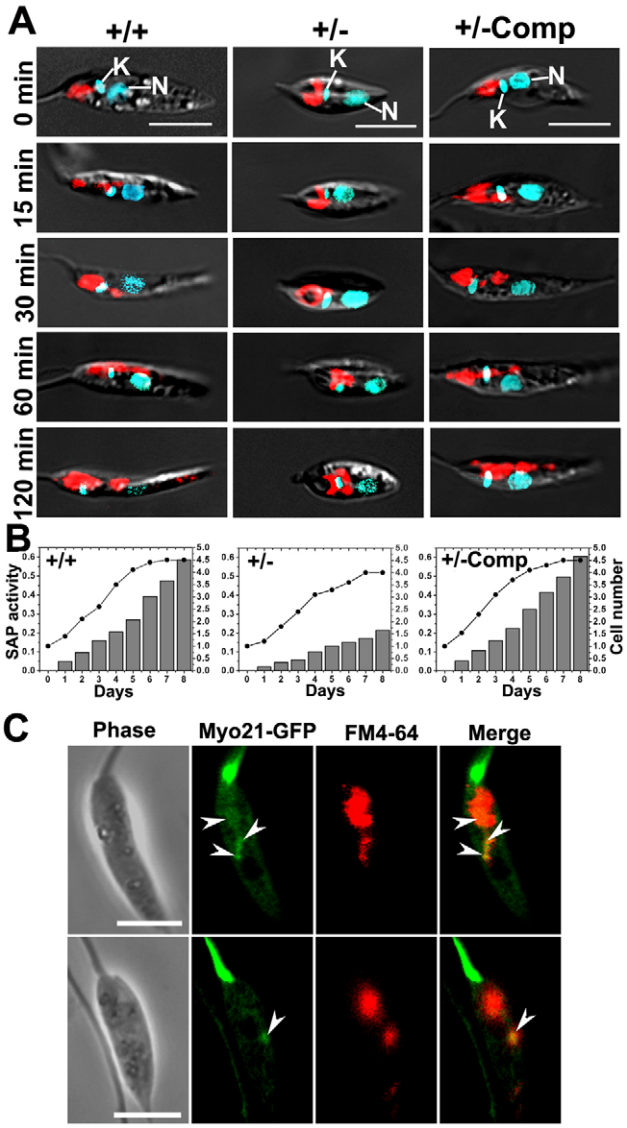

Fig. 7. Microscopic analysis of intracellular trafficking by assessing endocytic internalization of FM4-64. (**A**) Characteristic enlargement of flagellar pocket revealed by cup-shaped patterns of the dye (red) in *Myo21*$^{+/-}$ cells. Kinetoplast (K) and nucleus (N) stained with Hoechst 33342 (cyan) as intracellular markers. Scale bars: 5 µm. (**B**) Assessment of intracellular-trafficking activity by measuring exocytosed SAP activity (*p*NPP hydrolyzed per minute in 200 µl). Results of one of the two experiments are presented. Both the experiments showed similar trends of SAP activity. (**C**) Fluorescence microscopic images of Myo21-GFP-expressing live wild-type cells showing patterned presence of Myo21-GFP (green) with the endocytosed FM4-64 dye at 1 hour (red) trafficked beyond the flagellar pocket region (arrowheads). +/+, wild-type cells; +/–, *Myo21*$^{+/-}$ cells; +/–Comp, *Myo21*$^{+/-\text{Comp}}$ cells. Scale bars: 5 µm.

reduced with time, compared with levels in wild-type cells (Fig. 7B). However, these defects in intracellular trafficking were reversed to normal after episomal complementation. Together, these results clearly reveal that Myo21 is essentially required for intracellular trafficking in *Leishmania* cells.

To examine whether the reduced vesicular trafficking in *Myo21*$^{+/-}$ cells was due to the flagellar pocket abnormalities or due to the direct involvement of Myo21 in the intracellular transport, we incubated the live Myo21-GFP expressing cells for 1 hour with FM4-64 and then analyzed the incubated cells for association of Myo21 with the internalized dye (Fig. 7C). Interestingly, many cells that trafficked FM4-64 beyond the flagellar pocket, showed association of Myo21-GFP with the dye, indicating a direct involvement of Myo21 in the intracellular vesicle transport in *Leishmania* cells. However, our attempts to examine the association of actin with the vesicles containing dye, were not successful because of loss of FM4-64 in the cell-permeabilization step during the process of actin labeling with anti-actin antibodies (Sahasrabuddhe et al., 2004). Nevertheless, actin was also present in the regions where Myo21 associated with the dye (Fig. 1A; supplementary material Fig. S1).

Intracellular trafficking is impaired by disrupting actin dynamics

Single and double *Cof* gene mutants (*Cof*$^{+/-}$ and *Cof*$^{-/-}$) of *Leishmania* have been described to display phenotypic properties that are similar to those observed here with *Myo21*$^{+/-}$ mutants (Tammana et al., 2008). We therefore analyzed growth-dependent Myo21 expression (supplementary material Fig. S9A) and intracellular Myo21 localization (supplementary material Fig. S9B) in *Myo21*$^{-/-}$ cells. These experiments revealed that similarly to the *Myo21*$^{+/-}$ cells, Myo21 expression did not alter with the growth stage in these cells. The flagellar localization also remained unchanged despite the absence of actin in the flagellum. These results suggested that both Cof and Myo21 are required during assembly of the flagellum. Since depletion of Cof is known to severely impair actin dynamics (Tammana et al., 2008) and dynamic

actin is required in myosin-based intracellular trafficking (Zheng et al., 2009; Cramer, 2008; Semenova et al., 2008), we also analyzed vesicular transport in *Cof*$^{-/-}$ cells (supplementary material Fig. S9C). These mutants, similarly to *Myo21*$^{+/-}$ cells, exhibited considerably reduced vesicular transport, strongly suggesting an involvement of the actin-based intracellular-trafficking activity of Myo21 in assembly of the *Leishmania* flagellum. To further examine whether actomyosin activity was also required in the assembly of the IFT particles at the flagellar base, we immunolabeled both the *Myo21*$^{+/-}$ and *Cof*$^{-/-}$ cells for IFT172, using *T. brucei* IFT172 antibodies, which have been used as a marker of IFT in trypanosomes (Absalon et al., 2008). These antibodies intensely labeled the proximal flagellar region immediately below the region where Myo21 was concentrated in both the wild-type and mutant cells (Fig. 8), suggesting that Myo21 controls the IFT distribution in *Leishmania* cells. To test this possibility, we analyzed the IFT172 distribution in *Myo21*$^{+/-}$ cells that possessed relatively longer flagellum (supplementary material Fig. S10A). The IFT172 was distributed beyond the proximal flagellar location of Myo21 in these mutant cells, indicating that Myo21 does not control the IFT distribution in *Leishmania* flagellum. Furthermore, as the patterns of IFT172 staining in both the wild-type and mutant cells were similar (Fig. 8), we inferred that Myo21-mediated intracellular trafficking does not affect the assembly of the IFT particles at the flagellar base. This was confirmed when we observed similar expression levels of IFT172 in both wild-type and mutant cells in western blot analyses (supplementary material Fig. S10B).

Discussion

Most eukaryotes express several isoforms of myosin that perform diverse cellular functions. However, *Leishmania* cells express only a single myosin isoform, Myo21, which preferentially localizes at the proximal region of the flagellum (Katta et al., 2009). In the present study we show that Myo21 associates with actin and is indirectly involved in the flagellar length regulation. We further reveal that depletion of Myo21 results in impairment of flagellar assembly and intracellular trafficking. These abnormalities are, however, reversed by episomal complementation. In addition, we show that, similarly to *Myo21*-depleted cells, the flagellum assembly and intracellular trafficking are also impaired in the *Cof*-depleted cells. Together, these results indicate that the trafficking activity of Myo21 is essentially required in assembly of the *Leishmania* flagellum.

Eukaryotic cells are endowed with a well-coordinated intracellular trafficking system consisting of microfilament and microtubule tracks powered by myosin proteins, and kinesin and dynein motors, respectively (Ross et al., 2008). In the flagellar compartment, only kinesin and dynein microtubule-based motors have been implicated in cargo transport during flagellar assembly (Scholey, 2003; Cole and Snell, 2009). The flagellar cargoes associate with intraflagellar transport (IFT) complexes that are transported from the flagellar base to the flagellar tip (anterograde) and from the flagellar tip to the base (retrograde), respectively, by the kinesin and dynein motors (Rosenbaum and Witman, 2002). As the flagellar proteome consists of a plethora of proteins (more than 300) (Broadhead et al., 2006) and the number of cargoes associated with the IFT identified so far is limited, we propose that other mechanisms also operate in the transport system within the flagellum. An example in support of this proposal comes through an interesting study in which an IFT mutant of *T. brucei* showed movement of a subflagellar organelle, 'the flagella connector', beyond the axoneme microtubules, raising the possibility of a new form of intraflagellar transport besides the IFT (Davidge et al., 2006). Similarly, transport of PFR proteins in the flagellar compartment is also perplexing (Ralston and Hill, 2008), especially in induced IFT RNAi mutants of *T. brucei* (Absalon et al., 2008), conveying the gaps in our current knowledge of protein transport in the flagellar compartment. Bridging these observations is the example of the actin-based motor protein myosin VIIa, which

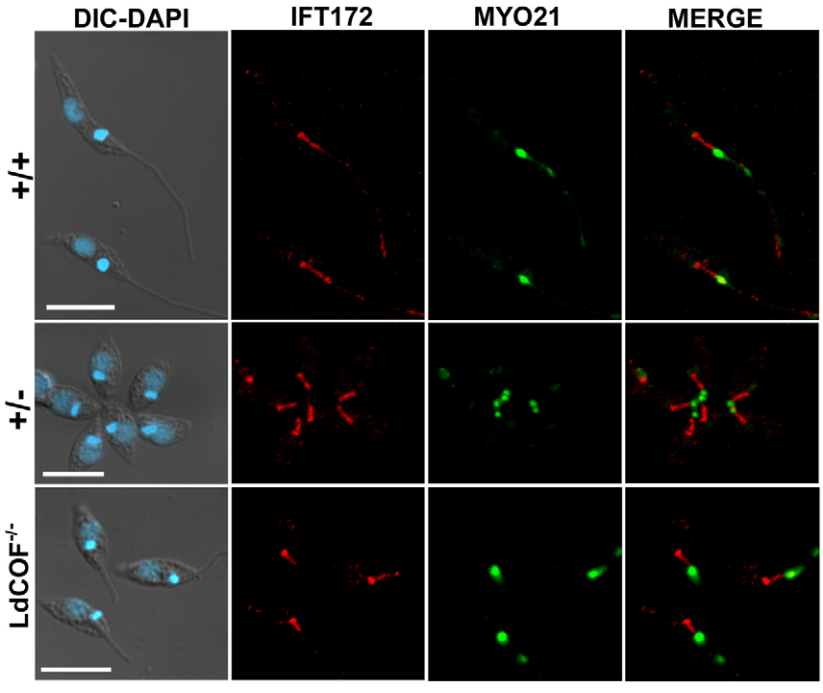

Fig. 8. Localization of IFT172 and Myo21 in *Leishmania* promastigotes. IFT172 and Myo21 in wild-type (*Myo21*$^{+/+}$), *Myo21*$^{+/-}$ and *Cof*$^{-/-}$ cells. Intensity of fluorescence signal is adjusted and images are not quantitative. Scale bars: 5 µm.

localizes in the connecting cilium, and is responsible for transport of 'opsin' from the inner to the outer segment of photoreceptor (Liu et al., 1997; Liu et al., 1999). Since the presence of actin in the flagella has already been reported in several eukaryotic organisms, including *Leishmania* (Muto et al., 1994; Yanagisawa and Kamiya, 2001; Minoura, 2005; Sahasrabuddhe et al., 2004; Broadhead et al., 2006), the flagellar localization of Myo21 and its association with actin indicate the possible role of the actomyosin system in the intraflagellar transport of protein cargoes.

Protein transport in relation to flagella formation can be segregated into two major steps: (1) transport of protein complexes from the cell body to the flagellar compartment, and (2) transport of these complexes along the flagellar length within this compartment. In the *Leishmania* flagellum, Myo21 localizes predominantly and stably at the proximal region, whereas rest of the flagellar Myo21 content is detergent labile. This means that the fixed and free Myo21 can interact with different protein entities, which could impart different functions to these two Myo21 subpopulations. At the proximal region, Myo21 is fixed through its tail domain (Katta et al., 2009), implying that the motor domain (head domain) is freely projected in the flagellar matrix. This organization would form a 'myosin-crew' in such a manner that its motor activity can propel actin and/or actin-bound cargoes into or out of the flagellar compartment depending upon their orientation in the crew. Earlier studies have shown that inhibition of anterograde IFT results in abrupt seizure of flagella formation owing to the lack of building blocks, whereas inhibiting retrograde IFT results in short swollen flagella filled with amorphous material, which fails to recycle to the flagellar base (Pedersen and Rosenbaum, 2008). The *Myo21*$^{+/-}$ mutant, which possesses a short flagellum, shows no accumulation of material in the flagellar compartment and appears to be largely an anterograde-transport-inhibition phenotype. It would therefore seem that the reduction in myosin level might have impeded the entry of some of the cargoes from the cell body to the flagellum. To some extent the 'myosin-crew' model explains how the reduction of Myo21 would have affected the transport of many flagellar components from the cell body to the flagellum, and consequently, generation of the short-flagella phenotype. Disruption of a putative retrograde transport motor, DHC2.2, in *L. mexicana* is known to result in the short-flagella phenotype, but in contrast to other cell types (Pazour et al., 1999; Wicks et al., 2000), it does not lead to accumulation of flagellar proteins in its short flagellum (Adhiambo et al., 2005). We therefore speculate that in addition to anterograde transport, Myo21 might also be involved in the retrograde transport of the flagellar proteins within the flagellar compartment.

It has been suggested that IFT cargoes assemble at the base of the flagellum before being transported within the flagellar compartment (Cole and Snell, 2009; Bloodgood, 2000). Indeed, presence of IFT172 in the rudimentary flagellum in both *Myo21*$^{+/-}$ and *Cof*$^{-/-}$ mutants suggests that assembly of IFT components is, in fact, not affected in these mutants. Nevertheless, it is possible that despite fully functional IFT-dependent transport, flagellum assembly is hampered because of the absence of components that are transported through the Myo21-dependent pathway. Alternatively, since flagellar elongation requires coordination of a number of interdependent signaling events (Rotureau et al., 2009), lack of key proteins transported through Myo21 might impede the cascade of flagella elongation and results in the short-flagella phenotypes, as observed in the present study. Furthermore, the detergent-soluble sub-fraction of Myo21 could be involved in the transport of proteins within the flagellum. It is, however, difficult to envisage at the moment whether this Myo21 subpopulation is part of the IFT or whether it forms a separate trafficking unit within the flagellum.

It has been reported that alterations in the lipid composition of the flagellar membrane hamper flagella formation (Tull et al., 2004). However, it is not yet clear whether axoneme assembly and the mobilization of lipid and protein components of the flagellar membrane are linked, or whether axoneme disassembly causes the concerted retrieval of the flagellar membrane (Cole and Snell, 2009). In the present study, Myo21 activity in membrane trafficking during endocytosis and exocytosis appear to link flagellar elongation with the addition of flagellar membrane and vice versa in trypanosomatids. The fact that Myo21 performs different functions at different locations raises the possibility of modulation in cargo recognition owing to post-translational modifications and/or other binding partners such as myosin heavy-chain kinases and calmodulin, both of which are encoded in the *Leishmania* genome. In addition, a distinct ubiquitin-associated domain at the C-terminus of Myo21 could also integrate extracellular signals and intracellular transport activities in these parasitic organisms.

Materials and Methods

Cell culture

L. donovani cells were maintained in high-glucose DMEM supplemented with 10% heat-inactivated fetal bovine serum and 40 μg/ml gentamycin at 25°C. To define the growth phases of *Leishmania* promastigotes, 10^5 cells/ml were seeded from the fully grown promastigote cultures and their growth was subsequently monitored by counting the cell numbers at 24 hour time intervals for at least 15 days. Cell growth was plotted on a log scale and early-log, mid-log and stationary phases were assigned in the curve (supplementary material Fig. S5). Sticking strictly to these growth conditions, the following parameters for early-log, mid-log and stationary phases of cell growth were used: 24-36 hours ($0.5\text{-}1\times10^6$ cells/ml) as early-log phase, 60-96 hours ($2\text{-}10\times10^6$ cells/ml) as mid-log phase and 12-14 days ($\sim4\times10^7$ cells/ml) as stationary phase. Although mutant cells grew a little more slowly, they were also harvested at the same time points.

Deletion, constructs and genetic manipulation

The 5′ and 3′ flanking sequences *Myo21* in *L. donovani* were determined using primer pairs F1, R1 and F2, R2 by PCR, as described earlier (Tammana et al., 2008). The amplicons were cloned in InsT/Aclone vector (TZ57R, MBI Fermentas), and sequenced and submitted to EMBL (accession numbers, 5′ flank, FM582168; 3′ flank, FM582169). To generate deletion cassettes, the 5′ flank was amplified using primers F3 and R3 and cloned in TZ57R vector and named 5flk/TZ57R. Similarly, the 3′ flank was amplified using primers F4 and R4, cloned in TZ57R vector and named 3flk/TZ57R. Then the 3′ flank was digested at *Nhe*I and *Bam*HI sites and ligated in the 5flk/TZ57R after digestion with the same set of restriction enzymes. This clone containing both the 5′ and 3′ flanks was named 5/3flk/TZ57R. The 5′-end of the 3′ flank contained *Nhe*I and *Not*I restriction sites, which were used for cloning of neomycin phosphotransferase (*Neo*) or hygromycin phosphotransferase (*Hyg*) genes. *Neo* and *Hyg* genes were amplified using F5, R5 and F6, R6 primer sets from pXG-GFP (a kind gift from Stephen M. Beverley) (Ha et al., 1996) and pCDNA3 vectors (Invitrogen) respectively, and cloned at *Nhe*I and *Not*I site of 5/3flk/TZ57R. Both *Hyg* and *Neo* genes were tagged with M-sequence (Debrabant et al., 1995) for improved expression of the *Neo* and *Hyg* genes. Transfection of *Leishmania* promastigotes was carried out by electroporation of the deletion cassette released by *Apa*I and *Xba*I digestion, as described earlier (Tammana et al., 2008). The *Myo21* single and double deletion mutants (*Myo21*$^{+/-}$ and *Myo21*$^{-/-}$) of *L. donovani* were selected against 10 μg/ml G-418 and/or 10 μg/ml hygromycin on DMEM-agar plates. Single colonies on the plates were carefully picked and inoculated in liquid medium with appropriate antibiotics. *Leishmania* ADF/cofilin (*Cof*) single and double deletion mutants were generated as described earlier (Tammana et al., 2008). See supplementary material Table S1 for all primer sequences.

Scanning and transmission electron microscopy

For scanning electron microscopy, cells were fixed with 4% paraformaldehyde and 1% glutaraldehyde in 0.1 M phosphate-buffered saline (PBS), pH 7.4, and the cell suspensions were placed on poly-L-lysine (0.1%)-coated coverslips and allowed to adhere for 45 minutes in a humid chamber. Cells were post fixed in 1% osmium tetroxide for 1 hour at room temperature and were dehydrated in an ascending series of ethanol, critical-point dried and coated with Au-Pd (80:20) using a sputter coater

(Polaron E 5000). Samples were examined in a Phillips DXL30 ESEM at an accelerating voltage of 30 kV. At least 200 cells were analyzed in each sample.

For transmission electron microscopy, cells were fixed with 1% glutaraldehyde in DMEM without FCS for 15 minutes at room temperature, sedimented and resuspended in 1% glutaraldehyde in PBS for 1 hour. After repeated washes with PBS, the cells were post-fixed with 1% OsO_4 in PBS at room temperature for 2 hours and wrapped in 2% low-melting agarose (Sigma). Small pieces of agarose-wrapped samples were subjected to dehydration using ethanol and acetone followed by additional staining with 1% uranyl acetate. Dehydrated samples were embedded in Epon-Araldite plastic mixture and polymerized at 60°C for 48 hours. Ultra-thin sections (50-70 nm) were picked up onto 200 mesh copper grids and were doubly stained with uranyl acetate and lead citrate. The sections were analyzed under a FEI Tecnai-12 Twin Transmission Electron Microscope equipped with a SIS Mega View-II CCD camera at 80 KV (FEI Company).

Antibodies, western blotting and immunofluorescence

Anti-Myo21 antibodies and anti-*Leishmania* actin antibodies were generated as described earlier (Katta et al., 2009; Sahasrabuddhe et al., 2004). Anti-PFR, anti-GRP78 and anti-IFT172 antibodies were a kind gift from Diane McMahon Pratt (Yale University, New Haven, CT), Emanuela Handman (Walter and Eliza Hall Institute of Medical Research, Melbourne, Australia) and Philippe Bastin (Pasteur Institute and CNRS, Paris, France), respectively. Antibodies against α- and β-tubulin were from Sigma. For western blotting, lysates of *Leishmania* promastigotes were prepared by washing the cells in PME buffer (0.1 M PIPES, 1 mM $MgCl_2$ and 1 mM EGTA) and boiling the washed cells in 1× SDS sample buffer. Protein samples (cell lysates, 40 µg/ lane) were resolved on SDS-PAGE and electroblotted on to a PVDF membrane. The blotted membranes were treated with blocking buffer (5% skimmed milk in PBS) and probed with the primary antibodies [actin, 1:10,000; Myo21, 1:1000; mAb10E2 (Ismach et al., 1989), 1:1000; GRP78 (Jensen et al., 2001), 1:100,000 and IFT172 (Absalon et al., 2008), 1:2000] diluted in blocking buffer. HRP-conjugated secondary antibodies (Santa Cruz) were used at 1:20,000 dilution. The protein bands were detected using Millipore chemiluminescent reagent and band intensities were measured using image master software.

For immunofluorescence microscopy, cells were washed with PBS and attached on glass coverslips coated with poly-L-lysine for 5 minutes at 25°C and then fixed with 4% (w/v) paraformaldehyde in PBS for 15 minutes. Fixed cells were permeabilized with 0.5% NP-40 and blocked with 0.1% BSA in PBS. For the preparation of the cytoskeleton, cells attached to the poly-L-lysine-coated coverslips were treated with 0.5% NP-40 in PME buffer for 15 minutes on ice, washed once with chilled PME buffer and then fixed with 4% (w/v) paraformaldehyde in PBS as above. Cells were treated with anti-Myo21 antibodies (1:1000), anti-actin antibodies (1:500) and/or anti-tubulin antibodies (1:1000) for 4 hours at 4°C and stained with Alexa Fluor 488- and Cy3-labeled secondary antibodies (1:1000). To label IFT172, cells on poly-L-lysine-coated coverslips were fixed for 5 minutes in methanol at –20°C, blocked in 0.1% BSA in PBS for 10 minutes (Absalon et al., 2008) and processed for labelling, as above. Image acquisition was done on ZEISS LSM510 META confocal system using a 63×, 1.4 NA (Oil) Plan Apochromate lens at 3× digital zoom and arranged in Adobe Photoshop (version 7.0). Since the fluorescence signal of Myo21 was very low in other regions of the cell body compared with the proximal region of the flagellum, immunofluorescence imaging was performed at relatively high gain settings in cases when Myo21 needed to be visualized clearly at other cellular locations.

Immunoprecipitation

Leishmania promastigotes (5×10^8) expressing Myo21-GFP, H-Myo21-GFP, T-Myo21-GFP (Katta et al., 2009), GFP alone (as control) or axenic amastigotes (5×10^8) expressing Myo21-GFP were lysed in chilled F-actin buffer (3.0 ml) containing 0.2 mM ATP, 0.2 mM $CaCl_2$, 2.0 mM $MgCl_2$, 100 mM KCl and 10 mM HEPES, pH 7.4, and 1% Triton X-100 (v/v) in the presence of 5.0 µg/ ml leupeptin, 0.1 mM PMSF, 10 µg/ ml N^{α}-tosyl-L-lysine chloromethyl ketone hydrochloride, 0.5 mM 4-(2-aminoethyl)benzenesulfonyl fluoride hydrochloride and 5.0 mM bezamidine hydrochloride. For immunoprecipitation analyses in amastigotes, axenic *Leishmania* amastigotes (5×10^8), expressing Myo21-GFP or GFP alone, were also lysed separately, as above. The lysates were centrifuged and the supernatants (3 ml) were mixed with 10 mg Protein-A-Sepharose beads (lyophilized, Amersham Pharmacia) rocking at 4°C for 30 minutes, followed by centrifugation. The clear supernatants were subjected to protein estimation and 2 µg anti-GFP antibodies (Invitrogen) were mixed with 1 ml lysates containing ~3 mg protein (promastigotes) and ~2.2 mg protein (amastigotes), and incubated for 30 minutes on ice. Antibody-antigen complexes were captured by adding 5 mg Protein-A-Sepharose beads (Amersham Pharmacia) and incubated while rocking for 30 minutes at 4°C, and washed six times with 1 ml chilled F-actin buffer. Proteins were liberated by boiling the beads in 200 µl SDS sample buffer for 5 minutes. 30 µl of these samples were subjected to SDS-polyacrylamide gel electrophoresis followed by western blotting.

Motility assessment by time-lapse microscopy

Motility measurements were performed on a Leica microscope DM5000B after collecting time-lapse movies for 36 seconds at 10× magnification. Paths of individual cells displayed on the time-lapse movie were traced manually on a transparency and scanned for presentation (Leica, Germany) as described earlier (Tammana et al., 2008). To show details of cell motility of the mutant cells, high-magnification movies were collected for ~35 seconds using an eyepiece camera 'CatCam130' and ScopePhoto software on the Zeiss Axioscope inverted microscope with 100× (oil emersion) DIC objective lens.

Intracellular trafficking

To assess the intracellular trafficking in *Leishmania*, endocytic vesicles were traced microscopically by using the fluorophore FM4-64, essentially as described (Sahin et al., 2008; Mullins et al., 2001). Briefly, *Leishmania* cells (5×10^6 cells/ml) were treated with FM4-64 dye in a microcentrifuge tube at 4°C for 10 minutes and the temperature was then raised to 25°C. Small aliquots (50 µl) were then harvested at different time intervals and mixed with 2% paraformaldehyde solution prepared in phosphate-buffered saline. To the fixed, labeled cells Hoechst 33342 dye was added at 10 µg/ml and the cells were immediately imaged under Zeiss LSM510 Meta confocal microscope using a 63×, 1.4 NA (OIL) Plan Apochromate lens and 3× digital zoom.

The exocytic activity was assessed by measuring SAP in the *Leishmania* culture medium at different time intervals, as described (Bakalara et al., 1995). Briefly, cells at 10^7 cells/ml density were resuspended in a 15 ml culture medium and 1 ml of the culture was harvested at 24 hour time intervals for 7 days. Cells were centrifuged and the supernatants were kept frozen at –80°C until use. The reaction was carried out in a total volume of 200 µl containing 100 µl culture supernatant and 50 mM Tris-HCl, pH 7.0, 0.1% (v/v) β-mercaptoethanol and 50 mM *p*-NPP. The reaction was stopped after 30 minutes by adding 800 µl of 0.25 M NaOH and absorbance of the *p*-nitrophenolate ion was measured at 410 nm. Results were presented as nanomoles of para-nitrophenyl phosphate (*p*-NPP) hydrolyzed per minute in a 0.2 ml reaction volume.

This work was partly supported by the research grant awarded to C.M.G. by the Department of Biotechnology, Government of India, New Delhi (India), under the Distinguished Biotechnology Research Professorship Scheme. We thank Stephen M. Beverley, Diane McMahon Pratt, Emanuela Handman and Philippe Bastin for providing pXG vectors, anti-PFR antibodies, anti-GRP78 antibodies and anti-IFT172 antibodies, respectively. S.S.K. and T.V.S.T. are the recipients of Research Fellowships from the Council of Scientific and Industrial Research, New Delhi (India). This is Communication No. 7895 from CDRI, Lucknow (India).

Supplementary material available online at
http://jcs.biologists.org/cgi/content/full/123/12/2035/DC1

References

Absalon, S., Blisnick, T., Kohl, L., Toutirais, G., Doré, G., Julkowska, D., Tavenet, A. and Bastin, P. (2008). Intraflagellar transport and functional analysis of genes required for flagellum formation in trypanosomes. *Mol. Biol. Cell* **19**, 929-944.

Adhiambo, C., Forney, J. D., Asai, D. J. and LeBowitz, J. H. (2005). The two cytoplasmic dynein-2 isoforms in Leishmania mexicana perform separate functions. *Mol. Biochem. Parasitol.* **143**, 216-225.

Allen, C. L., Goulding, D. and Field, M. C. (2003). Clathrin-mediated endocytosis is essential in *Trypanosoma brucei*. *EMBO J.* **22**, 4991-5002.

Bakalara, N., Seyfang, A., Baltz, T. and Davis, C. (1995). *Trypanosoma brucei* and *Trypanosoma cruzi*: life cycle-regulated protein tyrosine phosphatase activity. *Exp. Parasitol.* **81**, 302-312.

Bastin, P., Matthews, K. R. and Gull, K. (1996). The paraflagellar rod of Kinetoplastida: solved and unsolved questions. *Parasitol. Today* **12**, 302-307.

Bloodgood, R. A. (2000). Protein targeting to flagella of trypanosomatid protozoa. *Cell. Biol. Int.* **24**, 857-862.

Briggs, L. J., McKean, P. G., Baines, A., Moreira-Leite, F., Davidge, J., Vaughan, S. and Gull, K. (2004). The flagella connector of Trypanosoma brucei: an unusual mobile transmembrane junction. *J. Cell Sci.* **117**, 1641-1651.

Broadhead, R., Dawe, H. R., Farr, H., Griffiths, S., Hart, S. R., Portman, N., Shaw, M. K., Ginger, M. L., Gaskell, S. J., McKean, P. G. et al. (2006). Flagellar motility is required for the viability of the bloodstream trypanosome. *Nature* **440**, 224-227.

Cole, D. G. and Snell, W. J. (2009). SnapShot: Intraflagellar transport. *Cell* **137**, 784-784.

Cramer, L. (2008). Organelle transport: dynamic actin tracks for myosin motors. *Curr. Biol.* **18**, R1066-R1068.

Cruz, A. K., Titus, R. and Beverley, S. M. (1993). Plasticity in chromosome number and testing of essential genes in *Leishmania* by targeting. *Proc. Natl. Acad. Sci. USA* **90**, 1599-1603.

Cuvillier, A., Redon, F., Antoine, J. C., Chardin, P., DeVos, T. and Merlin, G. (2000). LdARL-3A, a *Leishmania* promastigote-specific ADP-ribosylation factor-like protein, is essential for flagellum integrity. *J. Cell Sci.* **113**, 2065-2074.

Cuvillier, A., Miranda, J. C., Ambit, A., Barral, A. and Merlin, G. (2003). Abortive infection of *Lutzomyia longipalpis* insect vectors by aflagellated LdARL-3A-Q70L overexpressing *Leishmania amazonensis* parasites. *Cell. Microbiol.* **5**, 717-728.

Davidge, J. A., Chambers, E., Dickinson, H. A., Towers, K., Ginger, M. L., McKean, P. G. and Gull, K. (2006). Trypanosome IFT mutants provide insight into the motor

location for mobility of the flagella connector and flagellar membrane formation. *J. Cell Sci.* **119**, 3935-3943.
Debrabant, A., Gottlieb, M. and Dwyer, D. M. (1995). Isolation and characterization of the gene encoding the surface membrane 3′-nucleotidase/nuclease of Leishmania donovani. *Mol. Biochem. Parasitol*. **71**, 51-63.
Desjeux, P. (2004). Leishmaniasis. *Nat. Rev. Microbiol*. **9**, 692.
Dumas, C., Ouellette, M., Tovar, J., Cunningham, M. L., Fairlamb, A. H., Tamar, S., Olivier, M. and Papadopoulou, B. (1997). Disruption of the trypanothione reductase gene of *Leishmania* decreases its ability to survive oxidative stress in macrophages. *EMBO J.* **16**, 2590-2598.
El-Sayed, N. M., Myler, P. J., Blandin, G., Berriman, M., Crabtree, J., Aggarwal, G., Caler, E., Renauld, H., Worthey, E. A., Hertz-Fowler, C. et al. (2005). Comparative genomics of trypanosomatid parasitic protozoa. *Science* **309**, 404-409.
Ersfeld, K. and Gull, K. (2001). Targeting of cytoskeletal proteins to the flagellum of *Trypanosoma brucei. J. Cell Sci.* **114**, 141-148.
Field, M. C. and Carrington, M. (2009). The trypanosome flagellar pocket. *Nat. Rev. Microbiol.* **7**, 775-786.
Foth, B. J., Goedecke, M. C. and Soldati, D. (2006). New insights into myosin evolution and classification. *Proc. Natl. Acad. Sci. USA* **103**, 3681-3686.
García-Salcedo, J. A., Pérez-Morga, D., Gijón, P., Dilbeck, V., Pays, E. and Nolan, D. P. (2004). A differential role for actin during the life cycle of *Trypanosoma brucei*. *EMBO J.* **23**, 780-789.
Ghedin, E., Debrabant, A., Engel, J. C. and Dwyer, D. M. (2001). Secretory and endocytic pathways converge in a dynamic endosomal system in a primitive protozoan. *Traffic*. **2,**175-188.
Ha, D. S., Schwarz, J. K., Turcob, S. J. and Beverley, S. M. (1996). Use of the green fluorescent protein as a marker in transfected *Leishmania*. *Mol. Biochem. Parasitol.* **77**, 57-64.
Hayashi, M., Hirono, M. and Kamiya, R. (2001). Recovery of flagellar dynein function in a Chlamydomonas actin/dynein-deficient mutant upon introduction of muscle actin by electroporation. *Cell Motil. Cytoskeleton*. **49**, 146-153.
Ismach, R., Cianci, C. M., Caulfield, J. P., Langer, P. J., Hein, A. and McMahon-Pratt, D. (1989). Flagellar membrane and paraxial rod proteins of *Leishmania*: characterization employing monoclonal antibodies. *J. Protozool.* **36**, 617-624.
Jensen, A. T., Curtis, J., Montgomery, J., Handman, E. and Theander, T. G. (2001). Molecular and immunological characterization of the glucose regulated protein 78 of *Leishmania donovani. Biochim. Biophys. Acta* **1549**, 73-87.
Karcher, R. L., Deacon, S. W. and Gelfand, V. I. (2002). Motor-cargo interactions: the key to transport specificity. *Trends Cell Biol.* **12**, 21-27.
Kato-Minoura, T., Hirono, M. and Kamiya, R. (1997). Chlamydomonas inner-arm dynein mutant, ida5, has a mutation in an actin-encoding gene. *J. Cell Biol*. **137**, 649-656.
Katta, S. S., Sahasrabuddhe, A. A. and Gupta, C. M. (2009). Flagellar localization of a novel isoform of myosin, myosin XXI, in *Leishmania. Mol. Biochem. Parasitol.* **164**, 105-110.
Kohl, L., Robinson, D. and Bastin, P. (2003). Novel roles for the flagellum in cell morphogenesis and cytokinesis of trypanosomes. *EMBO J*. **22**, 5336-5346
Krendel, M. and Mooseker, M. S. (2005). Myosins: tails (and heads) of functional diversity. *Physiology (Bethesda)*. **20**, 239-251.
Liu, X., Vansant, G., Udovichenko, I. P., Wolfrum, U. and Williams, D. S. (1997). Myosin VIIa, the product of the Usher 1B syndrome gene, is concentrated in the connecting cilia of photoreceptor cells. *Cell Motil. Cytoskeleton*. **37**, 240-252.
Liu, X., Udovichenko, I. P., Brown, S. D., Steel, K. P. and Williams, D. S. (1999). Myosin VIIa participates in opsin transport through the photoreceptor cilium. *J. Neurosci.* **19**, 6267-6274.
Minoura, T. K. (2005). Impaired flagellar regeneration due to uncoordinated expression of two divergent actin genes in *Chlamydomonas*. *Zool. Sci.* **22**, 571-577.
Moreira-Leite, F. F., Sherwin, T., Kohl, L., Gull, K. (2001). A trypanosome structure involved in transmitting cytoplasmic information during cell division**.** *Science* **294**, 610-612**.**
Mottram, J. C., McCready, B. P., Brown, K. G. and Grant, K. M. (1996). Gene disruptions indicate an essential function for the LmmCRK1 cdc2-related kinase of *Leishmania mexicana*. *Mol. Microbiol.* **22**, 573-583.
Mullin, K. A., Foth, B. J., Ilgoutz, S. C., Callaghan, J. M., Zawadzki, J. L., McFadden, G. I. and McConville, M. J. (2001). Regulated degradation of an endoplasmic reticulum membrane protein in a tubular lysosome in *Leishmania mexicana. Mol. Biol. Cell* **12**, 2364-2377.
Muto, E., Masaki, E., Masafumi, H. C. and Kamiya, R. (1994). Immunological detection of actin in the 14s ciliary dynein of *Tetrahymena*. *FEBS Lett.* **343**, 173-176.
Nayak, R. C., Sahasrabuddhe, A. A., Bajpai, V. K. and Gupta, C. M. (2005). A novel homologue of coronin colocalizes with actin in filament-like structures in *Leishmania*. *Mol. Biochem. Parasitol.* **143**, 152-164.
Odronitz, F. and Kollmar, M. (2007). Drawing the tree of eukaryotic life based on the analysis of 2,269 manually annotated myosins from 328 species. *Genome Biol.* **8**, R196.
Overath, P., Stierhof, Y.-D. and Wiese, M. (1997). Endocytosis and secretion in trypanosomatid parasites: tumultuous traffic in a pocket. *Trends Cell Biol.* **7**, 27-33.
Pazour, G. J., Dickert, B. L. and Witman, G. B. (1999). The DHC1b (DHC2) isoform of cytoplasmic dynein is required for flagellar assembly. *J. Cell Biol*. **144**, 473-481.
Pedersen, L. B. and Rosenbaum, J. L. (2008). Intraflagellar transport (IFT) role in ciliary assembly, resorption and signalling. *Curr. Top. Dev. Biol.* **85**, 23-61.
Ralston, K. S. and Hill, K. L. (2008). The flagellum of *Trypanosoma brucei*: new tricks from an old dog. *Int. J. Parasitol.* **38**, 869-884.
Rogers, M. E., Chance, M. L. and Bates, P. A. (2002). The role of promastigote secretory gel in the origin and transmission of the infective stage of *Leishmania mexicana* by the sandfly *Lutzomyia longipalpis*. *Parasitology*. **124**, 495-507.
Rosenbaum, J. L. and Witman, G. B. (2002). Intraflagellar transport. *Nat. Rev. Mol. Cell Biol.* **3**, 813-825.
Ross, J. L., Ali, M. Y. and Warshaw, D. M. (2008). Cargo transport: molecular motors navigate a complex cytoskeleton. *Curr. Opin. Cell Biol.* **20**, 41-47.
Rotureau, B., Morales, M. A., Bastin, P. and Späth, G. F. (2009). The flagellum-MAP kinase connection in Trypanosomatids: a key sensory role in parasite signaling and development? *Cell Microbiol.* Epub ahead of print.
Sahasrabuddhe, A. A., Bajpai, V. K. and Gupta, C. M. (2004). A novel form of actin in *Leishmania*: molecular characterisation, subcellular localisation and association with subpellicular microtubules. *Mol. Biochem. Parasitol.* **134**, 105-114.
Sahin, A., Espiau, B., Tetaud, E., Cuvillier, A., Lartigue, L., Ambit, A., Robinson, D. R. and Merlin, G. (2008). The *Leishmania* ARL-1 and Golgi traffic. *PLoS One*. **3**, e1620.
Santrich, C., Moore, L., Sherwin, T., Bastin, P., Brokaw, C., Gull, K. and LeBowitz, J. H. (1997). A motility function for the paraflagellar rod of Leishmania parasites revealed by PFR-2 gene knockouts. *Mol. Biochem. Parasitol*. **90,** 95-109.
Scholey, J. M. (2003). Intraflagellar transport. *Annu. Rev. Cell Dev. Biol.* **19**, 423-443.
Semenova, I., Burakov, A., Berardone, N., Zaliapin, I., Slepchenko, B., Svitkina, T., Kashina, A. and Rodionov, V. (2008). Actin dynamics is essential for myosin-based transport of membrane organelles. *Curr. Biol.* **28**, 1581-1586.
Tammana, T. V., Sahasrabuddhe, A. A., Mitra, K., Bajpai, V. K. and Gupta, C. M. (2008). Actin-depolymerizing factor, ADF/cofilin, is essentially required in assembly of *Leishmania* flagellum. *Mol. Microbiol.* **70**, 837-852.
Tovar, J., Wilkinson, S., Mottram, J. C. and Fairlamb, A. H. (1998). Evidence that trypanothione reductase is an essential enzyme in *Leishmania* by targeted replacement of the tryA gene locus. *Mol. Microbiol.* **29**, 653-660.
Tull, D., Vince, J. E., Callaghan, J. M., Naderer, T., Spurck, T., McFadden, G. I., Currie, G., Ferguson, K., Bacic, A. and McConville, M. J. (2004). SMP-1, a member of a new family of small myristoylated proteins in kinetoplastid parasites, is targeted to the flagellum membrane in *Leishmania*. *Mol. Biol. Cell* **15**, 4775-4786.
Wicks, S. R., de Vries, C. J., van Luenen, H. G. and Plasterk, R. H. (2000). CHE-3, a cytosolic dynein heavy chain, is required for sensory cilia structure and function in Caenorhabditis elegans. *Dev. Biol*. **221**, 295-307**.**
Woolner, S. and Bement, W. M. (2009). Unconventional myosins acting unconventionally. *Trends Cell Biol.* **19**, 245-252.
Yanagisawa, H. and Kamiya, R. (2001). Association between actin and light chains in *Chlamydomonas* flagellar innerarm dyneins. *Biochem. Biophy. Res. Comm.* **288**, 443-447.
Zakai, H. A., Chance, M. L. and Bates, P. A. (1998). In vitro stimulation of metacyclogenesis in *Leishmania braziliensis*, *L. donovani*, *L. major* and *L. mexicana*. *Parasitology*. **116**, 305-309.
Zheng, M., Beck, M., Müller. J., Chen, T., Wang, X., Wang, F., Wang, Q., Wang, Y., Baluska, F., Logan, D. C., et al. (2009). Actin turnover is required for myosin-dependent mitochondrial movements in *Arabidopsis* root hairs. *PLoS One*. **18**, e5961.